resulting relaxation of the SSH fields would force eastward-propagating and downwelling Kelvin waves which would deepen the eastern mixed layer and return the system to a normal configuration. These changes may be seen in the spring and early summer of 1998 in Fig. 1.

The results presented above suggest that the Indian Ocean exhibits strong coupled ocean–atmosphere–land interactions that are self-maintaining, and are capable of producing significant perturbations to the annual cycle, at least during the 1997–1998 period. Arguably, the evolution of the perturbation is independent of ENSO. We note that other hypotheses[3,4] have been suggested for observed interannual variability in the Indian Ocean. These theories rely on the Indian Ocean responding locally to either weaker or stronger monsoon winds which, through changes in upwelling and mixing, introduce a biennial component to the system. But the weakness of these theories is the maintenance of the upper-ocean anomalies from year to year. Our hypothesis adds a coupled dynamical component that has a longer timescale than the thermodynamics of the mixed layer, and which may form a link from one monsoon season to the next. Thus we suggest that the Indian Ocean may not be a passive player in climate variability on seasonal to interannual timescales, but may enact a very active and independent role. □

Received 6 July 1998; accepted 9 July 1999.

1. Nicholls, N. Air-sea interaction and the quasi-biennial oscillation. *Mon. Weath. Rev.* **106,** 1505–1508 (1983).
2. Nicholls, N. All-India summer monsoon rainfall and sea surface temperature around northern Australia and Indonesia. *J. Clim.* **8,** 1463–1467 (1995).
3. Meehl, G. A. Coupled ocean-atmosphere-land processes and south Asian monsoon variability. *Science* **265,** 263–267 (1994).
4. Meehl, G. A. The south Asian monsoon and the tropospheric biennial oscillation. *J. Clim.* **10,** 1921–1943 (1997).
5. Webster, P. J. & Palmer, T. N. The past and future of El Niño. *Nature* **390,** 562–564 (1997).
6. Reynolds, R. & Marisco, D. An improved real-time global sea surface temperature analysis. *J. Clim.* **6,** 114–119 (1993).
7. Kalnay, E. *et al.* The NCEP/NCAR 40-year reanalysis project. *Bull. Am. Meteorol. Soc.* **77,** 437–471 (1996).
8. Hendricks, J. R., Leben, R. R., Born, G. H. & Koblinsky, C. J. Empirical orthogonal function analysis of global TOPEX/POSEIDON altimeter data and implications for detection of global sea level rise. *J. Geophys. Res.* **101,** 14131–14145 (1996).
9. Yu, L. & Rienecker, M. M. Mechanisms for the Indian Ocean warming during the 1997–1998 El Niño. *Geophys. Res. Lett.* **26,** 735–738 (1999).
10. Barnett, T. P. Interaction of the monsoon and Pacific Ocean trade wind systems at interannual time scales. Part I: the equatorial zone. *Mon. Weath. Rev.* **111,** 756–773 (1983).
11. Arkin, P. & Meisner, B. The relationship between large-scale convective rainfall and cloud cover over the western hemisphere during 1982–1984. *Mon. Weath. Rev.* **115,** 51–74 (1987).
12. Webster, P. J. Response of the tropical atmosphere to local steady forcing. *Mon. Weath. Rev.* **100,** 518–541 (1972).
13. Gill, A. E. Some simple solutions for heat-induced tropical circulation. *Q. J. R. Meteorol. Soc.* **106,** 447–462 (1981).
14. *Near Real-Time Analysis of the Ocean and Atmosphere* Fig T 29, p. 36 (Climate Diagnostics Bull. NO. 97/11, Climate Diagnostics Center, National Center of Environmental Prediction, NOAA, Washington DC, 1997).
15. Gill, A. *Atmosphere-Ocean Dynamics* (Academic, London, 1982).
16. Webster, P. J. *et al.* Monsoons: processes, predictability and the prospects for prediction. *J. Geophys. Res.* **103,** 14451–14510 (1998).
17. Nicholson, S. E. & Kim, J. The relationship of the El-Niño Southern Oscillation to African rainfall. *Int. J. Climatol.* **17,** 117–135 (1997).
18. Nicholson, S. E. An analysis of the ENSO signal in the tropical Atlantic and western Indian Oceans. *Int. J. Climatol.* **17,** 345–375 (1997).
19. Reverdin, G., Cadet, D. & Gutzler, D. Interannual displacements of convection and surface circulation over the equatorial Indian Ocean. *Q. J. R. Meteorol. Soc.* **122,** 43–67 (1986).
20. Kapala, A., Born, K. & Flohn, H. in *Proc. Int. Conf. on Monsoon Variability and Prediction* (ed. Newson, R.) 119–126 (Tech. Doc. 619, World Meteorological Organization, Geneva, Switzerland, 1994).
21. Rao, K. G. & Goswami, B. N. Interannual variations of the sea-surface temperature over the Arabian Sea and the Indian Monsoon: A new perspective. *Mon. Weath. Rev.* **116,** 558–568 (1988).
22. Shukla, J. & Mooley, D. A. Empirical prediction of the summer monsoon over India. *Mon. Weath. Rev.* **115,** 695–703 (1987).

Supplementary information is available on *Nature*'s World-Wide Web site (http://www.nature.com) or as hard copy from the London editorial office of *Nature*.

Acknowledgements

This work was supported by the Office of Global Programs, NOAA, and the NSF (P.J.W., A.M.M., J.P.L.), and by NASA (R.R.L.).

Correspondence and requests for materials should be addressed to P.J.W. (e-mail: pjw@oz.colorado.edu).

A dipole mode in the tropical Indian Ocean

N. H. Saji*, B. N. Goswami†, P. N. Vinayachandran* & T. Yamagata*‡

** Institute for Global Change Research, SEAVANS N 7F, 1-2-1 Shibaura, Minato-ku, Tokyo 105 6791, Japan*
† Center for Atmospheric and Oceanic Sciences, Indian Institute of Science, Bangalore 560 012, India
‡ Department of Earth and Planetary Physics, Graduate School of Science, The University of Tokyo, Tokyo 113 0033, Japan

For the tropical Pacific and Atlantic oceans, internal modes of variability that lead to climatic oscillations have been recognized[1,2], but in the Indian Ocean region a similar ocean–atmosphere interaction causing interannual climate variability has not yet been found[3]. Here we report an analysis of observational data over the past 40 years, showing a dipole mode in the Indian Ocean: a pattern of internal variability with anomalously low sea surface temperatures off Sumatra and high sea surface temperatures in the western Indian Ocean, with accompanying wind and precipitation anomalies. The spatio-temporal links between sea surface temperatures and winds reveal a strong coupling through the precipitation field and ocean dynamics. This air–sea interaction process is unique and inherent in the Indian Ocean, and is shown to be independent of the El Niño/Southern Oscillation. The discovery of this dipole mode that accounts for about 12% of the sea surface temperature variability in the Indian Ocean—and, in its active years, also causes severe rainfall in eastern Africa and droughts in Indonesia—brightens the prospects for a long-term forecast of rainfall anomalies in the affected countries.

The catastrophic rains of 1961 in tropical eastern Africa and subsequent abrupt discharge of the White Nile are now known[4–6] to be part of an anomalous climate state over the tropical Indian Ocean. A dipole structure characterized the sea surface temperature (SST) anomaly during this event: warmer than usual SSTs occurred over large parts of the western basin, while SSTs off Sumatra were cooler than usual. Rainfall increased over tropical eastern Africa and the western Indian Ocean, while over the Indonesian archipelago it decreased, resulting in severe drought. Equatorial surface winds, which in a normal summer season blow towards the east, weakened and reversed direction. There was no El Niño in the Pacific, while India experienced the highest summer monsoon rainfall in the past 150 years (ref. 5). By examining long-term data sets of SST

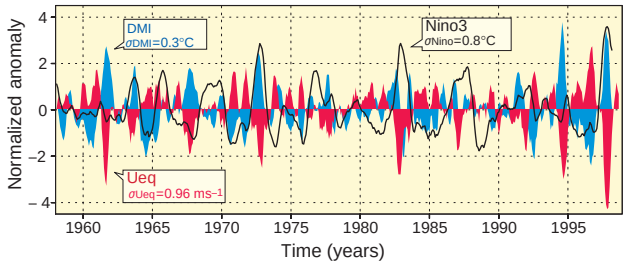

Figure 1 Dipole mode and El Niño events since 1958. Plotted in blue, the dipole mode index (DMI) exhibits a pattern of evolution distinctly different from that of the El Niño, which is represented by the Nino3 sea surface temperature (SST) anomalies (black line). On the other hand, equatorial zonal wind anomalies U_{eq} (plotted in red) coevolves with the DMI. All the three time series have been normalized by their respective standard deviations. We have removed variability with periods of 7 years or longer, based on harmonic analysis, from all the data sets used in this analysis. In addition, we have smoothed the time series using a 5-month running mean.

and surface winds we found several occurrences of these patterns. These observations motivated this study. However, here we use the GISST2.3b data set[7] (1958–98), the NCEP surface winds reanalysis[8] (1958–98) and the Xie–Arkin rainfall analyses[9] (1979–98) to present our findings, as the essential signatures of this phenomenon are unchanged in the various data sets we have examined.

Basin-scale anomalies of uniform polarity cover[3] the tropical Indian Ocean basin during El Niño/Southern Oscillation (ENSO) events. Using empirical orthogonal function (EOF) analysis we see that this pattern (EOF1) explains about 30% of the total variation of anomalous Indian Ocean SSTs. Next, the dipole mode (EOF2) explains about 12%. Characteristic to the dipole mode is a reversal in sign of SST anomaly across the basin. This reversal is so striking, that the dipole mode may be identified by a simple index time series which describes the difference in SST anomaly between the tropical western Indian Ocean (50° E–70° E, 10° S–10° N) and the tropical south-eastern Indian Ocean (90° E–110° E, 10° S–Equator). The strong correlation (>0.7) between this index, referred to as the dipole mode index (DMI), and the time series associated with EOF2 indicates the accuracy of the DMI in representing the dipole mode in SST.

The dipole mode event is independent of the ENSO in the Pacific Ocean. To demonstrate this, we plot SST anomalies representative of the central and eastern equatorial Pacific (from the so-called Nino3 region) against the DMI time series in Fig. 1. Note the significant dipole mode events of 1961, 1967 and 1994 coinciding with no ENSO, a La Niña and a weak El Niño, respectively. There are years in which dipole mode events coincide with strong ENSO events as in 1972 or 1997. We note here that the correlation between the DMI and Nino3 SST anomaly time series is weak (<0.35).

During dipole mode events, the surface wind field over the tropical Indian Ocean experiences large changes, especially in its zonal (east-to-west) component over the Equator. Maximum changes in the zonal wind occur over the equatorial central and eastern Indian Ocean, where we noted a correlation maximum of $> |0.6|$ with the DMI. By plotting the area-averaged equatorial zonal wind anomalies (U_{eq}) over this region (70° E–90° E, 5° S–5° N), in Fig. 1, we demonstrate that the intensity of the SST dipole mode and the strength of the zonal wind anomaly over the Equator are strongly dependent on each other.

Seasonal phase locking is an important characteristic of the DMI time series. Thus significant anomalies appear around June, intensify in the following months and peak in October. Because of this systematic seasonality of phase it is meaningful to demonstrate the evolution of a dipole mode event using composite analysis. We analysed the recent six extreme events of 1961, 1967, 1972, 1982, 1994 and 1997 to present the life cycle of a typical dipole mode event in Fig. 2. Cool SST anomalies first appear in the vicinity of the Lombok strait by May–June, accompanied by moderate south-easterly wind anomalies in the southeastern tropical Indian Ocean. In the following months, the cold anomalies intensify and appear to migrate towards the Equator along the Indonesian coastline, while the western tropical Indian Ocean begins to warm up. Zonal wind anomalies along the Equator and alongshore wind anomalies off Sumatra intensify together with the SST dipole. A dramatically rapid peaking of these features occurs in October, following by a rapid demise. The composite time series shown in Fig. 3 illustrates this sudden change of the DMI and U_{eq} more clearly. A strong feature in the time series is the tight coupling between the zonal wind anomaly and the dipole intensity. A biennial tendency—in this case a tendency for a dipole mode event to be preceded by an event of the opposite polarity—is evident. Note that the biennial tendency of U_{eq} is already well known[10]. Figure 3 also indicates that a pile-up of warm water off the Sumatran coast, together with westerly wind anomalies over the central-eastern equatorial Indian Ocean[11,12], signals the occurrence of a dipole mode event in the following year.

Basin-wide data for rainfall is available only since 1979. Analyses of the rainfall data (or proxy data sets such as outgoing longwave radiation) reveal that during a dipole mode event rainfall decreases over the oceanic tropical convergence zone (OTCZ) and increases over the western tropical Indian Ocean (Fig. 4). This pattern of rainfall is dynamically consistent with the convergence/divergence shifts associated with the wind field in the composite maps. Thus what emerges here is strong empirical evidence for coupling between the SST and the wind field through the precipitation field. Based on knowledge about the climate system in the Indian Ocean and from our own studies with a variety of modelling devices, we present the following model for how these fields are connected to each other.

In a normal year southeast trade winds converge into the South Equatorial Trough[13] associated with the high-rainfall (>10 mm d^{-1}) OTCZ. When, during a dipole mode event, SSTs off Sumatra begin cooling, convection weakens at the OTCZ and the consequent surface pressure modification (not shown) makes the southeast trade winds extend and converge further downstream. This altered large-scale wind field enhances convergence and moisture supply at the extended downstream end of the trade winds, thereby

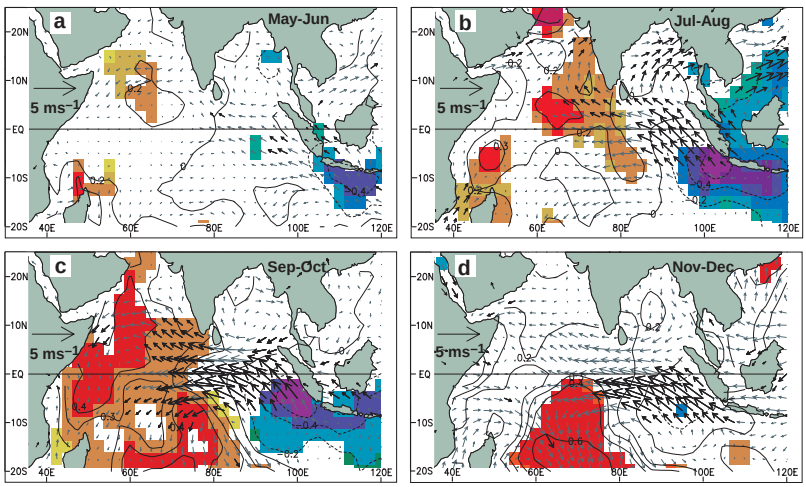

Figure 2 A composite dipole mode event. **a**–**d**, Evolution of composite SST and surface wind anomalies from May–June (**a**) to Nov–Dec (**d**). The statistical significance of the analysed anomalies were estimated by the two-tailed *t*-test. Anomalies of SSTs and winds exceeding 90% significance are indicated by shading and bold arrows, respectively.

encouraging precipitation northwest of the normal position of the OTCZ. These abnormally extended trade winds also interrupt the normal heat supply to the coast off Sumatra. In a normal summer monsoon season, the westerly winds along the Equator accumulate warmer water along this coast through downwelling equatorial and coastally trapped Kelvin waves[11,12,14]. The strongest manifestation of this process, occurring twice a year during monsoon transitions, is known as the Yoshida–Wyrtki Jet[11]. This process counters the cooling tendencies by evaporation, coastal upwelling and oceanic heat advection brought about by the strong alongshore winds off this coast. In a year with a dipole mode event, abnormally extended trade winds with an easterly component along the Equator, by preventing the intrusion of the equatorial current[15,16], allow the cooling processes to dominate off Indonesia. This cooling is further enhanced as entrainment processes associated with the coastal winds become more effective due to the shallower thermocline[17,18]. The shallowing thermocline is manifested in the observed lowering of the sea level[16–20]. Hydrographic observations in this region also favour the above model of the coupling between surface winds and SST through ocean dynamics[21]. The warming in the west is initiated as a consequence of this chain of cause and effect taking place in the eastern half. The shifting trade winds, by increasing convergence in the west, lead to reduced wind speed and reduced evaporation[18,20] which aid in warming up the SST. Entrainment is inhibited as increased rainfall raises the stability of surface waters through reduced salinity[18]. The thermocline anomalously deepens owing to reduced eastward transport[11,22] resulting from the altered trade winds. The warmer SST increases the precipitation anomaly and consequently the wind anomaly to its east, thus introducing a positive feedback mechanism. The see-saw of the thermocline implied in the above discussion of the dipole mode mechanism is supported by the see-saw in both sea level[16–20] and annual mean subsurface temperature anomalies[23] (not shown).

Here we have described a chain of events, which once initiated keeps the SST cooler in the tropical southeastern Indian Ocean, warmer in the tropical western Indian Ocean, and the southeast trade winds in the eastern half stronger than normal throughout the boreal summer and autumn. At this stage, the ocean–atmosphere system in the Indian Ocean approaches the configuration of those in the Pacific and Atlantic oceans[24], and presumably would have attained a similar state had it not been for the rapid demise of the instability after the boreal autumn. Our preliminary understanding indicates that it is the changes in the state of the climate system, brought about by the seasonal monsoonal reversals, that are responsible for the demise of the dipole mode event. The main factor influencing the instability is the cooler-than-normal SST off Sumatra. Because the mass and heat transport from the west, achieved through equatorial ocean dynamics, play an important role in the heat balance of this region, its fluctuations affect the SST. However, after the boreal autumn, until the next spring, weakening winds both along the Equator and along the coast diminish the importance of ocean dynamics in the regulation of SST. Consequently, fluctuations of the mass and heat transport caused by equatorial dynamics play a lesser role in SST fluctuations. On the other hand, the increased insolation (as a result of the seasonal movement of the Sun) and reduced evaporation (due to decreasing windspeeds) dominate the changes in SST in this region during this season. In this context, it is likely that the higher-than-normal insolation, due to the reduction or absence of cloudiness in the tropical southeastern Indian Ocean, acting on the thin mixed layer, returns the system back to normality by removing the cool SST anomaly.

As the dipole mode is strongly dependent on the state of the system set up by the monsoonal circulation, it is expected that the variability of the monsoons would significantly affect this mode. We note that the dipole mode shares certain common features, such as the biennial tendency[25], with the monsoonal variability. Also, easterly anomalies along the Equator as well as reduced convection in the OTCZ are well-known features of strong monsoons[26]. Nevertheless, the statistical correlation of the DMI with precipitation over the Asian monsoon regime does not yield a significant relationship (Fig. 4). Therefore the relationship of the DMI to the Indian monsoon variability is still not clear. It is clear, however, that the dipole mode has important implications for climate variability in other regions surrounding the Indian Ocean. The shift of the convergence zone, which leads to floods in east Africa and drought in Indonesia (Fig. 4), manifest the weakening or reversal of the zonal (Walker) circulation across the Indian Ocean. Besides causing this very discernible local climate variability across the basin, the zonal

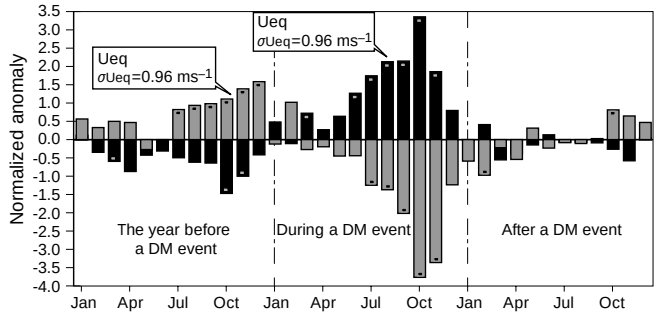

Figure 3 Strong coupling of SST dipole intensity to U_{eq}. Shown is the coevolution of intensity of the dipole mode (DMI, black bars) and strength of equatorial zonal winds anomalies (U_{eq}, grey bars) from the year before, to the year following a typical dipole mode event. Bars indicating significant anomalies (estimated by a two-tailed *t*-test) exceeding a 90% confidence level are marked with spots.

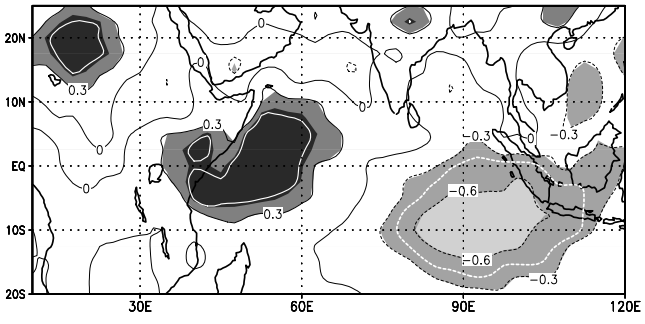

Figure 4 Rainfall shifts northwest of the OTCZ during dipole mode events. The map correlates the DMI and rainfall to illustrate these shifts. The areas within the white curve exceed the 90% level of confidence for non-zero correlation (using a two-tailed *t*-test).

redistribution of atmospheric mass and non-adiabatic heating during a dipole mode event may result in such an event influencing the countries surrounding the Indian Ocean through atmospheric teleconnections, as evidenced by the northward shift of the Pacific Subtropical High off the Philippines which caused an unusually hot summer in the far east Asian countries in 1994 (refs 27, 28). Some atmospheric general circulation model experiments[29,30] have demonstrated the important effects of the Indian Ocean SST changes on east African rainfall variability. Further experiments with atmospheric and oceanic models, extended in scope, will be needed to understand the full implications of this hitherto unexplored mode of climate variability. The dipole mode event should also provide a testing ground for coupled ocean–atmosphere models. □

Received 27 April; accepted 27 July 1999.

1. Neelin, J. D. *et al*. ENSO theory. *J. Geophys. Res. C* **103,** 14261–14290 (1998).
2. Zebiak, S. E. Air–sea interaction in the equatorial Atlantic region. *J. Clim.* **6,** 1567–1586 (1993).
3. Wallace, J. M. *et al*. On the structure and evolution of ENSO-related climate variability in the tropical Pacific. *J. Geophys. Res.* **103,** 14241–14260 (1998).
4. Flohn, H. East African rains of 1961/62 and the abrupt change of the White Nile discharge. *Palaeoecol. Afr.* **18,** 3–18 (1987).
5. Kapala, A., Born, K. & Flohn, H. in *Proc. Int. Conf. on Monsoon Variability and Prediction* 119–126 (Int. Centre for Theoretical Physics, Trieste, 1994).
6. Reverdin, G., Cadet, D. L. & Gutzler, D. Interannual displacements of convection and surface circulation over the equatorial Indian Ocean. *Q. J. R. Meteorol. Soc.* **112,** 43–67 (1986).
7. Rayner, N. A., Horton, E. B., Parker, D. E., Folland, C. K. & Hackett, R. B. *Version 2.2 of the Global Sea-Ice and Sea Surface Temperature Data Set, 1903–1994* (Clim. Res. Tech. Note 74, UK Meteorological Office, Bracknell, 1996).
8. Kalnay, E. *et al*. The NCEP/NCAR 40-year reanalysis project. *Bull. Am. Meteorol. Soc.* **77,** 437–471 (1996).
9. Xie, P. & Arkin, P. A. Analyses of global monthly precipitation using gauge observations, satellite estimates and numerical model predictions. *J. Clim.* **9,** 840–858 (1996).
10. Barnett, T. P. Interaction of the Monsoon and Pacific Trade Wind System at interannual time scales. Part I: The equatorial zone. *Mon. Weath. Rev.* **111,** 756–773 (1983).
11. Wyrtki, K. An equatorial jet in the Indian Ocean. *Science* **181,** 262–264 (1973).
12. Yamagata, T., Mizuno, K. & Masumoto, Y. Seasonal variations in the equatorial Indian Ocean and their impact on the Lombok throughflow. *J. Geophys. Res.* **101,** 12465–12474 (1996).
13. Stout, J. E. & Young, J. A. Low-level monsoon dynamics derived from satellite winds. *Mon. Weath. Res.* **111,** 774–799 (1983).
14. Clarke, A. J. & Liu, X. Observations and dynamics of semiannual and annual sea levels near the eastern equatorial Indian Ocean boundary. *J. Phys. Oceanogr.* **23,** 386–399 (1993).
15. Reppin, J., Schott, F. A., Fischer, J. & Quadfasel, D. Equatorial currents and transports in the upper central Indian Ocean: Annual cycle and interannual variability. *J. Geophys. Res.* (in the press).
16. Vinayachandran, P. N., Saji, N. H. & Yamagata, T. Response of the equatorial Indian Ocean to an unusual wind event during 1994. *Geophys. Res. Lett.* **26,** 1613–1616 (1999).
17. Behera, S. K., Krishnan, S. & Yamagata, T. Anomalous air–sea coupling in the southern tropical Indian Ocean during the boreal summer of 1994. *Geophys. Res. Lett.* (in the press).
18. Murtugudde, R., McCreary, J. P. & Busalacchi, A. J. Oceanic processes associated with anomalous events in the Indian Ocean with relevance to 1997–1998. *J. Geophys. Res.* (in the press).
19. Potemra, J. & Lukas, R. Seasonal to interannual modes of sealevel variability in the western Pacific and eastern Indian Oceans. *Geophys. Res. Lett.* **26,** 365–368 (1999).
20. Yu, L. S. & Rienecker, M. M. Mechanisms for the Indian Ocean warming during the 1997–98 El Niño. *Geophys. Res. Lett.* **26,** 735–738 (1999).
21. Meyers, G. Variation of Indonesian throughflow and the El Niño–Southern Oscillation. *J. Geophys. Res.* **101,** 12255–12263 (1996).
22. Hastenrath, S., Nicklis, A. & Greischar, L. Atmospheric-hydrospheric mechanisms of climate anomalies in the western equatorial Indian Ocean. *J. Geophys. Res.* **98,** 20219–20235 (1993).
23. Levitus, S., Boyer, P. & Antonov, J. *World Ocean Atlas*, Vol. 5, *Interannual Variability of Upper Ocean Thermal Structure.* (NOAA Atlas NESDIS, NODC/NOAA, Silver Spring, Maryland, USA, 1994).
24. Xie, S.-P. & Philander, S. G. H. A coupled ocean-atmosphere model of relevance to the ITCZ in the eastern Pacific. *Tellus A* **46,** 340–350 (1994).
25. Goswami, B. N. A multiscale interaction model for the origin of the tropospheric QBO. *J. Clim.* **8,** 524–534 (1995).
26. Goswami, B. N., Krishnamurthy, V. & Annamalai, H. A broad scale circulation index for the interannual variability of the Indian summer monsoon. *Q. J. R. Meteorol. Soc.* **125,** 611–633 (1999).
27. Kawamura, R., Sugi, M., Kayahara, T. & Sato, N. Recent extraordinary cool and hot summers in east Asia simulated by an ensemble climate experiment. *J. Meteorol. Soc. Jpn.* **76,** 597–617 (1998).
28. Nitta, T. Abnormal hot summer of 1994 and tropical convective activity. *Weath. Serv. Bull./Jpn. Meteorol. Agency* **63** (suppl.), 178–187 (1996) (in Japanese).
29. Goddard, L. & Graham, N. E. The importance of the Indian Ocean for simulating rainfall anomalies over eastern and southern Africa. *J. Geophys. Res.* (in the press).
30. Latif, M., Dommenget, D. & Dima, M. The role of Indian Ocean sea surface temperature in forcing east African climate anomalies. *J. Clim.* (in the press).

Acknowledgements

We thank H. Nakamura, Y. Masumoto, S. Behera and Y. Tanimoto for comments and discussions, and H. Watanabe and M. Yoshinaga for assistance in plotting the data.

Correspondence and requests for materials should be addressed to T.Y. (e-mail: yamagata@geoph.s.u-tokyo.ac.jp).

Tribosphenic mammal from the North American Early Cretaceous

Richard L. Cifelli

Oklahoma Museum of Natural History and Department of Zoology, University of Oklahoma, Norman, Oklahoma 73019, USA

The main groups of living mammals, marsupials and eutherians, are presumed to have diverged in the Early Cretaceous[1], but their early history and biogeography are poorly understood. Dental remains have suggested that the eutherians may have originated in Asia[2], spreading to North America in the Late Cretaceous, where an endemic radiation of marsupials was already well underway[3]. Here I describe a new tribosphenic mammal (a mammal with lower molar heels that are three-cusped and basined) from the Early Cretaceous of North America, based on an unusually complete specimen. The new taxon bears characteristics (molarized last premolar, reduction to three molars) otherwise known only for Eutheria among the tribosphenic mammals. Morphometric analysis and character comparisons show, however, that its molar structure is primitive (and thus phylogenetically uninformative), emphasizing the need for caution in interpretation of isolated teeth. The new mammal is approximately contemporaneous with the oldest known Eutheria from Asia. If it is a eutherian, as is indicated by the available evidence, then this group was far more widely distributed in the Early Cretaceous than previously appreciated. An early presence of Eutheria in North America offers a potential source for the continent's Late Cretaceous radiations, which have, in part, proven difficult to relate to contemporary taxa in Asia.

Class Mammalia

Infralegion Tribosphenida, Order and Family Uncertain

Montanalestes keebleri gen. et sp. nov.

Etymology. Montana: the state of origin; lestes (Greek): robber; *keebleri*: in honour of the Keebler family of Billings, Montana, in recognition of its support for field parties of the Oklahoma Museum of Natural History (OMNH).

Holotype. OMNH 60793, associated dentaries with right p3–5, m1–3 (terminology follows ref. 4), and alveoli for p2; and left p5, m1–3 (Fig. 1).

Locality and Horizon. OMNH V1156, basal unit VII (ref. 5), Cloverly Formation (Aptian–Albian; ~110 Myr); Carbon County, Montana, USA.

Diagnosis. Differs from primitive Tribosphenida (for example, *Kermackia*), in so far as is known, in having a semimolarized last premolar (lingually placed paraconid, incipient talonid basin, metaconid present) and only three molars; molars differ in having a broader, more fully basined talonid with three cusps consistently present. Differs from early marsupials and marsupial-like taxa[6] in postcanine tooth formula and in having semimolarized last premolar and a smaller size differential between m1–2; lower molars differ in lacking a labial postcingulid and in having a greater trigonid–talonid height differential, narrower talonid and a hypoconulid that is not lingually situated. Differs from *Slaughteria*[7] in having a semimolarized, less anteroposteriorly compressed last premolar; molars differ in having a smaller size differential between m1–2, no lingual knob on anterocingulid, more acute trigonid angle on m1 and taller paraconid relative to metaconid. Similar to early Eutheria in postcanine tooth formula (four or more premolars, three molars) and semimolarized last premolar; differs from most comparable taxon, *Prokennalestes*[8], in having salient lingual cingulids on the lower premolars and stronger paraconid and metaconid on p5, the former more lingually placed. Lower molars differ from those of *Prokennalestes* in having sequential length